Three-Dimensional Flow Modeling of a Self-wiping Corotating Twin-Screw Extruder. Part I

Goffart, D.; Wal, D.J. van der; Klomp, E.M.; Hoogstraten, H.W.; Janssen, L.P.B.M.; Breysse, L.; Trolez, Y.

Published in:
Polymer Engineering & Science

DOI:
10.1002/pen.10478

Three-Dimensional Flow Modeling of a Self-Wiping Corotating Twin-Screw Extruder. Part I: The Transporting Section

D. GOFFART,[1] D. J. VAN DER WAL,[2] E. M. KLOMP,[3] H. W. HOOGSTRATEN,[3] L. P. B. M. JANSSEN,[2]* L. BREYSSE,[1] *and* Y. TROLEZ[1]

[1]*Elf Aquitaine (Atochem), C.e.r.d.a.t.o 27470 Serquigny, France*

[2]*Department of Chemical Engineering University of Groningen Nijenborgh 4, 9747AG Groningen, The Netherlands*

[3]*Department of Mathematics University of Groningen 9700AV Groningen, The Netherlands*

A three-dimensional modeling of the transporting elements in a self-wiping corotating twin-screw extruder has been carried out by using the finite element package Sepran (1). This simulation uses the 3D geometry of the channel rolled over the twin-screw, which consists of the intermeshing and normal areas. The flow profile, the backflow volume, the pressure buildup, the shear and elongation rates, and the adiabatic axial temperature gradient have been calculated by solving the Navier-Stokes equations and the continuity equation for a Newtonian fluid. These results are given for different extruder parameters such as the throughput of the extruder, the rotation speed of the screws and the helix angle of the screws to better understand the influence of different extruder configurations. This study belongs to a program of research on the self-wiping corotating twin-screw extruder that also includes the modeling of the kneading elements (Part II) and, in the future, the study of scale-up and heat transfer.

INTRODUCTION

Twin-screw extruders are used extensively in polymer processing. The transporting elements are generally considered for the action of building of pressure, which pushes the polymer through the kneading elements, and the heating of polymers. In the twin-screw extruder, the channel of the transporting elements is interrupted by the flights of the other screw. The intermeshing zone is therefore of importance in the mixing. The self-wiping intermeshing twin-screw extruder is very attractive because of its wiping action, which provides the elimination of the dead material areas. An increase of pressure buildup is also noted. It is often said, but not proved, that elongation affects the process more than shear. The extruder parameters influence the process optimization, the residence time distribution, and the screw design. It is therefore necessary to calculate the flow profile to find the shear and elongation rates, the axial (down-channel) pressure gradient, and the backflow and to see how these parameters vary with rotation speed, throughput, helix angle, and viscosity. The shear rate greatly influences the temperatures in the extruder since one of the main sources of temperature generation is viscous dissipation.

Various studies of flow in intermeshing corotating twin-screw extruders have been published. These are summarized in a paper by Wang and White (2). In the present work, a 3D modeling of a fully filled channel from the transporting elements (*Fig. 1*) is used to simulate the flow patterns of a Newtonian fluid. In order to have realistic results the geometry is not unrolled and includes the specifics of the channel geometry in the intermeshing area of the twin-screw extruder. The screw is supposed fixed, while the barrel moves. One of the difficulties in the transporting elements is the interpretation of the throughput. The throughput of

* To whom correspondence should be addressed.

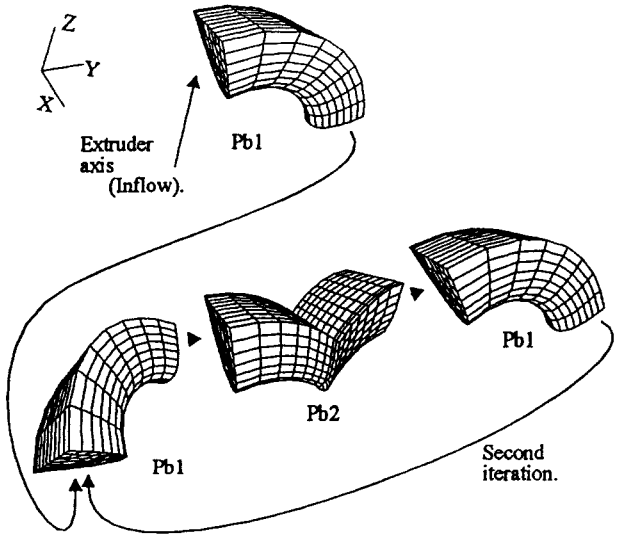

Fig. 1. 3D iteration process involving Pb1 and Pb2 and computational mesh (ϕ = 10.9°).

the extruder is equal to the prescribed amount of material fed by the hopper per second. The velocity of the material transported in the channel is also influenced strongly by the dragging forces from the rotation of the screw. Therefore there is a difference between the throughput of the extruder Q (perpendicular to a cross section of the extruder) and of the channel Q_c (perpendicular to a cross section of the channel) because a variation of the rotation speed or of the helix angle changes the throughput in the channel, Q_c, but not in the extruder, Q (See *Fig. 2* and the subsection on the throughput in the **Results and Discussion** section). In our approach, the development of the pressure follows from the given throughput, rotation speed, and extruder parameters. Consequently, we chose to relate the graphs of the results to Q, but it must be kept in mind that all values concern the channel (except for the buildup of pressure and the temperature rise). The effects resulting from the variation of the rotation speed and the throughput for two different helix angles and a backward element are considered. The influence of the viscosity is also studied. The discussion concerns the velocity profiles, the pressure buildup, and the elongation and shear rates in the channel of the extruder. Because of the complexity of the complete process in a twin-screw extruder, some assumptions are necessary, which are explained in the next two sections.

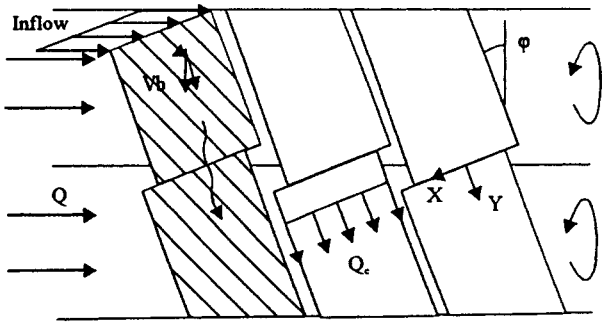

Fig. 2. The channel in the extruder.

As far as we know, no work dealing with a 3D simulation of the channel rolled over the screw for the transporting elements has yet been published.

MATHEMATICAL METHOD

In the simulation, the model is stationary and there are no body forces, so the equations (with 3D Cartesian coordinates) for isothermal laminar flow of an incompressible Newtonian liquid are:

$$\textit{conservation of mass: } div\ \vec{v} = 0 \tag{1}$$

$$\textit{momentum equations: } \rho(\vec{v}\cdot\nabla)\vec{v} + \nabla p = div\ t \tag{2}$$

with the velocity $\vec{v}$, the pressure p, and Newtonian fluid stress tensor $t = \eta(\nabla\vec{v} + \nabla\vec{v}^T)$.

Equations 1 and *2* are discretized. The Penalty method [Cuvelier *et al.* (3)] is used for the discretization of the incompressibility constraint. The idea of this method is to perturb the continuity equation with a small term containing the pressure:

$$\epsilon p + div\ \vec{v} = 0 \tag{3}$$

with ϵ a small parameter. The main advantage of this construction is that p can be eliminated from the momentum equations. Thus the calculations of the velocity and the pressure are now separated.

After discretization by Galerkin's method, the nonlinear equations for the solution of stationary laminar flow of incompressible liquids are:

$$S\vec{u} + N(\vec{u})\vec{u} - \frac{1}{\epsilon}L^T M_p^{-1} L\vec{u} = 0 \tag{4}$$

$$\vec{p} = -\frac{1}{\epsilon}M_p^{-1} L\vec{u} \tag{5}$$

with S the stress matrix, $\vec{u}$ the vector of unknown velocities, $N(\vec{u})\vec{u}$ the discretization of the convective terms, L the divergence matrix, M_p the pressure mass matrix and $\vec{p}$ the vector of unknown pressure values. In the numerical solution process, the nonlinear terms in *Eqs 4* and *5* are linearized (Picard linearization and Newton iteration).

To solve the 3D Navier-Stokes equations, the Sepran finite element package uses a triquadratic isoparametric brick element (Cartesian coordinates). The velocity is approximated by a full triquadratic approximation based on the 27 nodes from an element. The pressure is approximated linearly and is discontinuous. The numerical error in the velocity results decreases quadratically with the mesh size, but the results for the pressure are only first-order accurate [see Cuvelier *et al.* (3)]. However, the finite-element mesh used in our computations has been chosen sufficiently fine to guarantee satisfactory overall accuracy. We emphasize that the penalty function method is particularly suitable for our study since it allows the extruder throughput to be prescribed, whereas the

required pressure drop follows from the computations.

DEFINITION OF THE PROBLEM

Geometry and Mesh

The 2D geometry of a cross section is based on an adaptation of Booy's (4) results by Denson and Hwang (5), who modified Booy's expression to account for the effect of helix angle ϕ and who included a term to account for the flight width. Therefore, the cross section is defined by equations that give the variation of the channel depth without clearance. In the 3D geometry used, the curvature of the screw and barrel have not been neglected.

To simulate the complete channel of the transporting elements an iterative process with two different geometric problems was developed as shown in *Fig. 1*. The calculations are done successively for problems Pb1, Pb1, Pb2, Pb1, Pb1, Pb2, etc. This process allows us to use a minimum number of elements and enables us to extend the length of the channel as far as we want. As shown in *Figs. 1* and *2* (with V_b the velocity tangent to the barrel) a throughput is fixed at the inflow of the first Pb1 with the same direction as the extruder axis. In this process, the values are taken at the end of each geometric problem and transferred to the beginning of the following. The first Pb1 is not included in the iterative process because it is only used to establish an entry flow profile for the subsequent iterations.

Pb1 represents a quarter of one screw rotation and Pb2 the intermeshing area with two channels shifted in order to model the zigzag motion of the fluid when it passes from one screw to the other. Note that in Pb2 the cross sections along the channel are parallel and not perpendicular to the curved axis as for Pb1, thus facilitating the generation of a computational grid for Pb2. In the intermeshing region of the corotating twin-screw extruder the flight of one screw blocks part of the channel of the other screw. This small part of the cross-sectional geometry as used in our modeling is shown in *Fig. 3*, where it is depicted separately from the remaining cross-sectional mesh.

The geometric parameters employed in this simulation are:

1. the centerline distance of the twin-screw extruder $C_L = 40$ (mm).
2. the radius of the screw $R_s = 25$ (mm).
3. the number of screw threads $n = 2$.
4. the helix angle with two cases $\varphi = 10.9°$ [$\Leftrightarrow l = 30.2$ (mm)], and $\varphi = 14.3°$ [$\Leftrightarrow l = 40.1$ (mm)] with l the lead of the screw element. The helix angles tested were deliberately taken small to correspond to what is usually used in front of the kneading elements.

Assumptions and Boundary Conditions

The assumptions made in this simulation are the following:

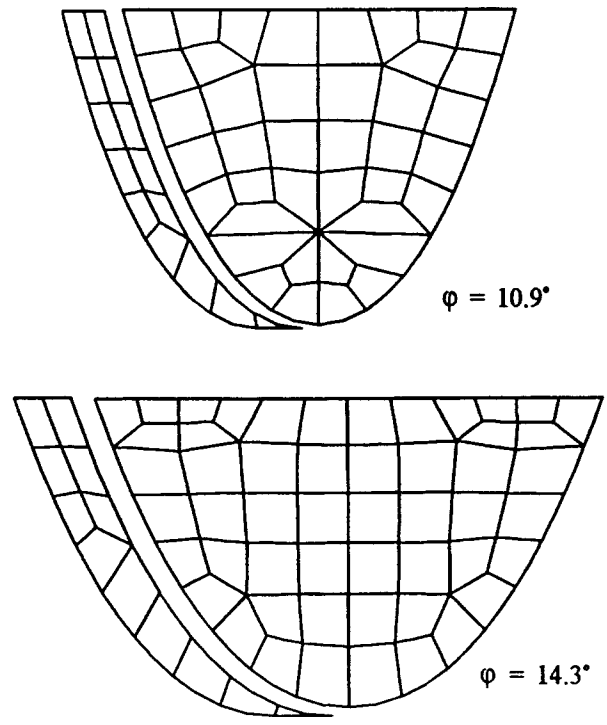

Fig. 3. 2D finite element mesh of the cross sections of the channel. For clarity, the small part of the cross section blocked by the flight of the other screw is shown separately.

A1. The assumptions concerning the geometry (see **Geometry and Mesh**).

A2. The space between the screw and the barrel is neglected, therefore the leakage is neglected. Davis (6) gives equations to compute the maximum shear rate located between the flight outer diameter and barrel diameter.

A3. The channel is fully filled, which can be considered realistic for the part of the screw placed before the kneading elements, before the backward transporting elements or before the die (7,8).

A4. The flow is a stationary, isothermal, and laminar flow of an incompressible Newtonian liquid. No body forces are prescribed. Although the Newtonian model is an obvious simplification for many situations occurring in practice, it is expected to provide a valuable first insight into the flow phenomena. Non-Newtonian fluid behavior will be incorporated in our future work.

A5. The rotation speed has a tangential direction to the barrel having an angle to the channel axis (φ).

The boundary conditions used are the following:

B1. A throughput Q_c is imposed on the plane inflow velocity profile of the first Pb1 before the iteration (see **Geometry and Mesh**).

B2. A velocity V_b (related to the rotation speed N as seen in *Fig. 2*) is prescribed on the barrel. On the screw surface and the small part of the mesh representing the screw flight that is blocked, see *Fig. 3*, the velocity is taken zero.

B3. A free-stress condition is imposed at the outflow plane [Cuvelier *et al.* (3)].

RESULTS AND DISCUSSION

Results will be presented for the flow profile, the pressure, the shear, and elongation rates, while varying the throughput and the rotation speed for a fixed geometry. This is done for two different helix angles. Because of a good convergence of the computations and of a fast establishment of the flow profile in the first Pb1, only one iteration was sufficient. The values for N are 50, 150, 300, and 400 (rpm) and for Q 5, 30, and 100 (ml/s). A backward transporting element is also presented with N varying, Q = 30 (ml/s), and φ = 10.9°. The influence of the viscosity is treated in the last section.

The Throughput

The two throughputs Q_c and Q_e are given in *Table 1* for each of the two helix angles considered. Q_e corresponds to the calculated extruder throughput, which is slightly different from the prescribed throughput Q because of the numerical discretization. Note that Q_c varies when Q_e is constant because N varies. Indeed, the rotational speed imposed on the barrel has a component parallel to the axis of the channel, which contributes to the general throughput in the channel. The axis of the extruder is perpendicular to V_b, therefore, N has no effect in the calculation of Q_e. The values of Q_c can be represented by the following functions:

$$Q_c[ml/s] = 8.04 \times 10^{-3} * N + 1.115 \times 10^{-2} * Q \quad \text{for} \quad \varphi = 10.9° \quad (6)$$

$$Q_c[ml/s] = 8.60 \times 10^{-3} * N + 1.927 \times 10^{-2} * Q \quad \text{for} \quad \varphi = 14.3° \quad (7)$$

There are two reasons why Q_c increases with φ. If φ is larger, the direction of the velocity given at the inflow is closer to the channel axis. Moreover, the area of the channel cross section increases with φ.

The Flow Profile

In *Figs. 4 a* and *b*, 3D plots of the axial velocity profiles are shown, for several cross-sections, along the axis of the channel for N = 150 (rpm), Q = 30 (ml/s), and φ = 10.9° (with *A* the inflow, *B* the intermeshing area, and *C* the outflow). These pictures give an idea of the shape of the flow profile. Although it remains almost the same along Pb1, this is not the case for Pb2 where some changes appear in the intermeshing zone. Here there is a small additional backflow just before the flight blocked area of the first screw and just after the flight blocked area of the second screw. These localized phenomena correspond to an axial recirculation in these zones. While ap-

Table 1. The Throughputs Q_e and Q_c for Various Values of N and φ.

N...Q...	Q_e (ml/s) φ = 10.9°	Q_c (ml/s) φ = 10.9°	Q_e (ml/s) φ = 14.3°	Q_c (ml/s) φ = 14.3°
N50Q5	4.58	0.46	4.62	0.53
N50Q30	27.5	0.74	27.7	1.01
N50Q100	91.7	1.52	92.5	2.36
N150Q5	4.58	1.26	4.62	1.39
N150Q30	27.5	1.54	27.7	1.87
N150Q100	91.7	2.32	92.6	3.22
N300Q5	4.58	2.47	4.62	2.68
N300Q30	27.5	2.75	27.7	3.16
N300Q100	91.7	3.53	92.5	4.51
N400Q5	4.58	3.28	4.62	3.54
N400Q30	27.5	3.56	27.7	4.02
N400Q100	91.7	4.34	92.5	5.37

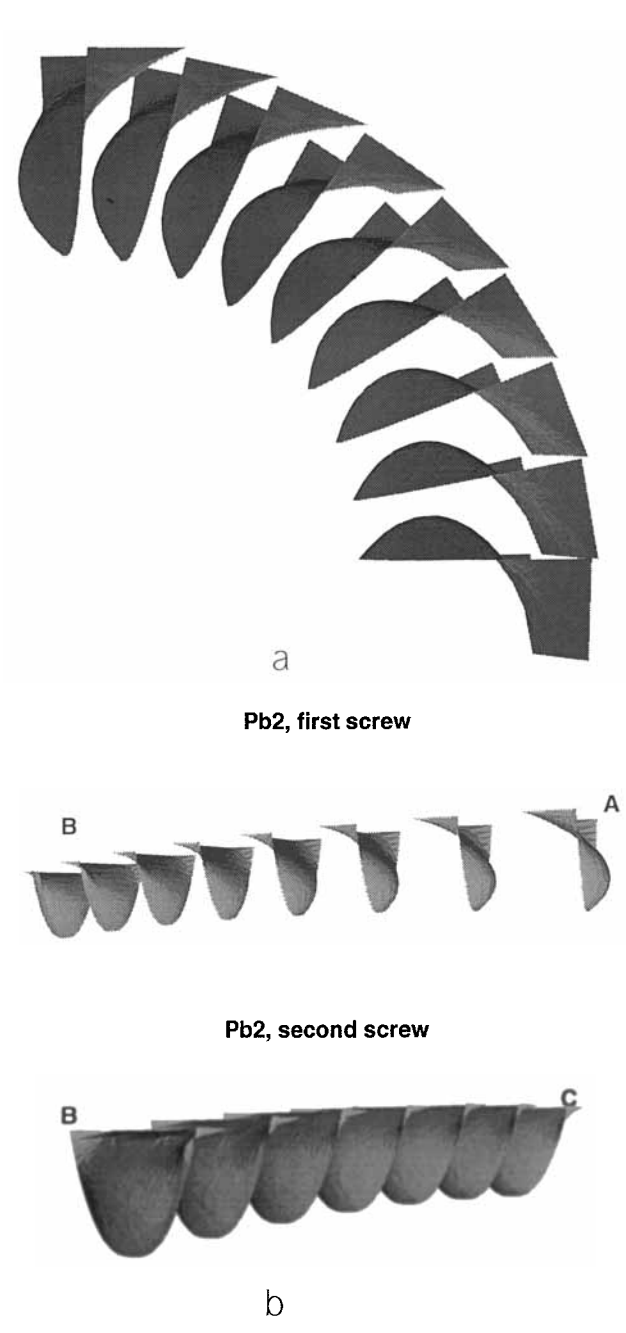

Fig. 4a. 3D visualization of the flow profile for Pb1 (N = 150 [rpm], Q = 30 [ml/s] and φ = 10.9°). Fig. 4b. 3D visualization of the flow profile for Pb2 (N = 150 [rpm], Q = 30 [ml/s] and φ = 10.9°). A: inflow, B: intermeshing area, C: outflow.

proaching the intermeshing area, the profile of the axial backflow becomes flatter. In *Fig. 5*, the vector plots in Pb2 (XZ plane) are given (with cross section no. 4, the middle), which show transverse recirculation in the cross sections. The vectors on the barrel increase as they are close to the middle, because the angle between the curve of the barrel and the cross section decreases. In *Fig. 6*, the axial outflow profile changes because an increase of Q reduces the negative area and the values of the backflow. When N is enlarged and Q constant, the negative area increases as well as the values of the axial velocities, because an increase of N augments Q_c and enlarges the axial recirculation. *Figure 7* presents the vector plots along the length of Pb2 (plane YZ) according to three sections, which give an idea of the axial component of the recirculation. A part of the axial recirculation is provoked by the shift of the channels, when the fluid particles pass from one screw to the other (*Fig. 2*). The total recirculation is not axial but oblique or helicoidal because of the helix angle.

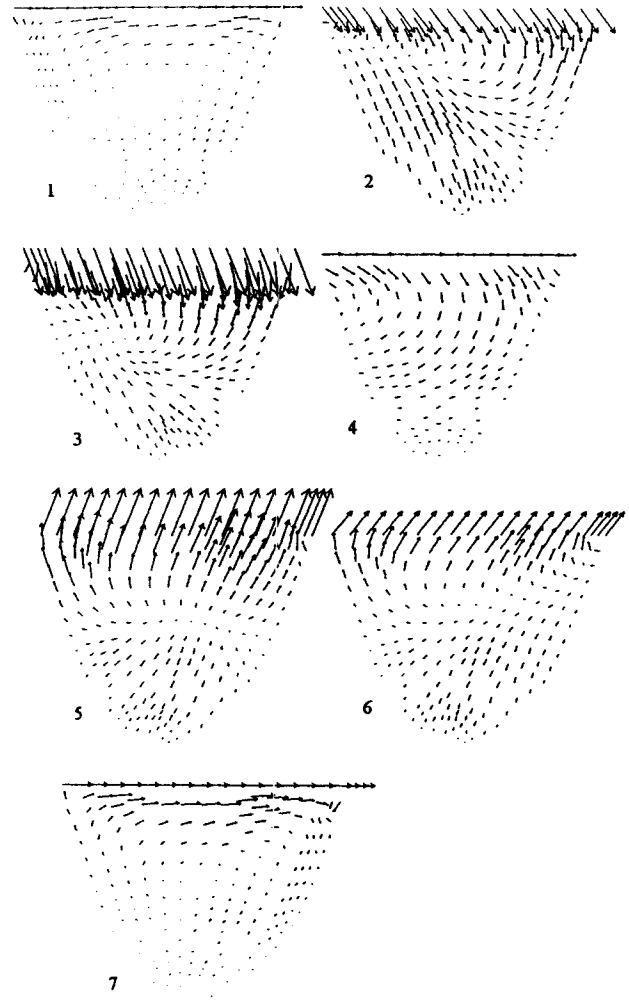

Fig. 5. Vector plots of transverse velocities in the cross sections of Pb2 (N = 150 [rpm], Q = 30 [ml/s] and φ = 10.9°) (1: inflow y = −15; 2: y = −10; 3: y = −3; 4: middle y = 0; 5: y = 3; 6: y = 10; 7: outflow y = 15 = R_s–H [mm]).

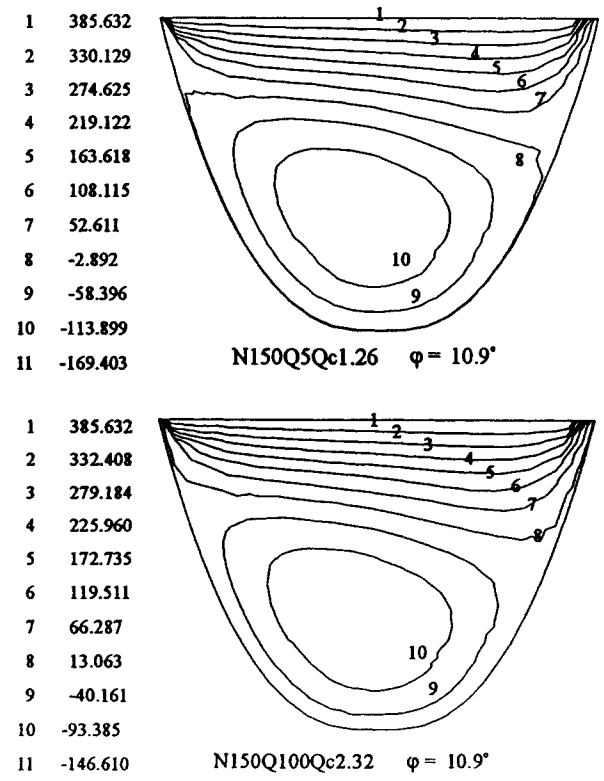

Fig. 6. Contour plots of the velocity perpendicular to the cross section for two cases.

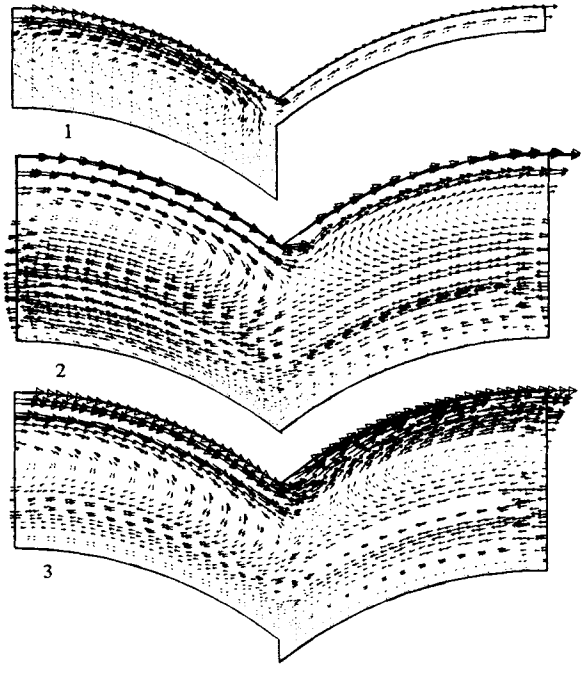

Fig. 7. Velocity vector plots for sections along length of Pb2 (N = 150 [rpm], Q = 30 [ml/s] and φ = 10.9°).

The Backflow

The backflow plays a prominent part in the mixing. The previous section has already referred to it, and the next discussion will concentrate on the relative back-

flow volume B^*, which is defined as minus the integral, over a cross section, of the amount of flow volume in the opposite direction (divided by Q_c). As can be seen in *Fig. 8*, B^* remains almost constant along Pb1, and its absolute value decreases in the intermeshing area as do the absolute values of the minimum and maximum axial velocities. One could think that this is provoked by the fact that the backflow is computed perpendicular to the cross sections, which are, for Pb2, parallel to each other. This point was checked by computing the backflow, for each cross section, perpendicular to the curve of the barrel. The results gave a reduction, even stronger, of the absolute value of B^* in the intermeshing area. Indeed, *Fig. 7* (as *Fig. 5*) shows that the vectors are smaller in this zone and that their direction is closer to the perpendicular of the cross section than to the tangent to the barrel (or screw) in the cross section.

The absolute value $|B^*|$, in *Fig. 9*, decreases when Q increases and/or N decreases. The curves of $|B^*|$ converge to a maximum when N increases. This maximum will be reached faster as Q is smaller because Q takes less and less importance compared to N. A comparison of both helix angles gives $|B^*|$ larger for the larger φ. This shows that the rotation speed plays a prominent part in B^*. Indeed, when φ is smaller, the transverse component of V_b (see *Fig. 2*) becomes smaller and so, there is less recirculation. It also explains why the difference in $|B^*|$ between both φ values increases with N in *Fig. 9*. The backward elements give larger values of $|B^*|$ for the same configurations. The difference between backward and forward elements remains constant. The values of B^* are represented by the following functions:

$$B^* = \frac{B}{Q_c} = \frac{-2.99 \times 10^{-2} * N + 8.52 \times 10^{-3} * Q}{8.04 \times 10^{-3} * N + 1.115 \times 10^{-2} * Q}$$

for $\varphi = 10.9°$ (8)

$$B^* = \frac{B}{Q_c} = \frac{-4.37 \times 10^{-2} * N + 1.71 \times 10^{-2} * Q}{8.60 \times 10^{-3} * N + 1.927 \times 10^{-2} * Q}$$

for $\varphi = 14.3°$ (9)

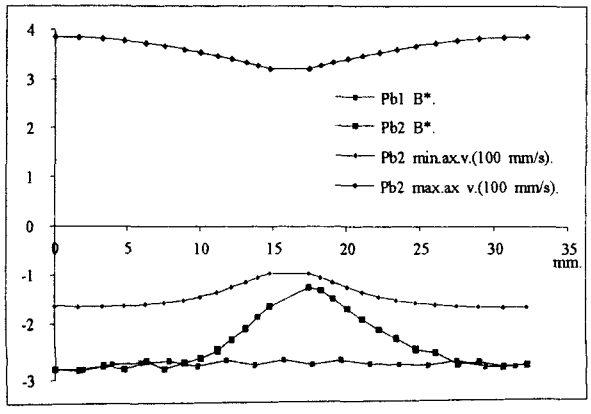

Fig. 8. The axial velocity and B^* along the channel (N = 150 [rpm], Q = 30 [ml/s] and φ = 10.9°).

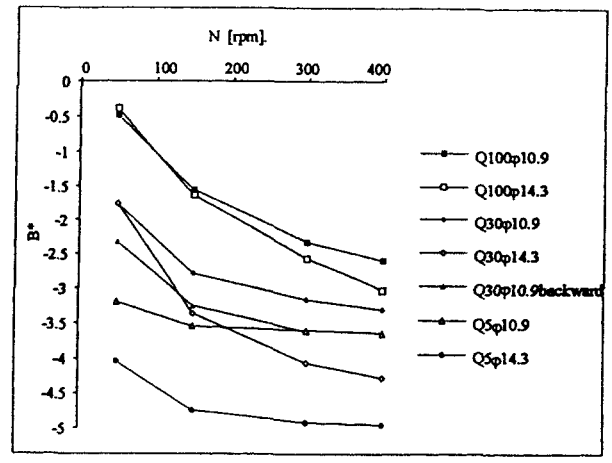

Fig. 9. B^* as a function of N for various values of Q and φ.

The equation:

$$B^* = -3.29 \times 10^{-3} * N - 7.32 \times 10^{-3}$$

for $Q = 30$ [ml/s] and $\varphi = 10.9°$ (10)

is fitted for the backward element.

For comparison, two cases with the same value of N/Q are observed (N = 50, Q = 5, and N = 300, Q = 30 with φ = 10.9°). They have almost the same values for B^*, respectively -3.189 and -3.164. For these cases $N_1/N_2 = Q_1/Q_2 = 6$, and B is respectively -1.463 and -8.708 (ml/s) where the ratio is the same, 6. Therefore the relation between Q and N is $N_1 = (Q_1/Q_2)\ N_2$. As the Reynolds number is small, the solution is comparable with the solution of the Stokes equation (linear in the velocity) and therefore, a multiplication of the boundary conditions leads to a multiplication of all velocities and thus of B^* by the same factor. (All these remarks are also applicable to other helix angles).

The Axial Pressure Gradient

The pressure is important to consider, in order to calculate the build-up of pressure before the kneading elements. The increase of pressure, ΔP, per unity of length of the extruder (P is computed as the integral of the local pressure p over a cross-section divided by the area) is considered. The buildup of pressure taken separately along Pb1 and Pb2 is approximately the same.

Figure 10 shows the influence of N and Q on ΔP for the transporting elements along the extruder (Pb1). ΔP is influenced more by N than Q, but one has to keep in mind that Q_c is a function of N and Q. For larger values of Q than those used in this paper, there is no backflow anymore and a negative pressure gradient may occur. The larger φ will be, the smaller ΔP will be, which is one of the reasons why small φ is used before the kneading elements and the die. Indeed, when the cross section of the channel is smaller (φ smaller) the material requires a larger ΔP to move forward. The assumption of a fully filled screw channel is realistic

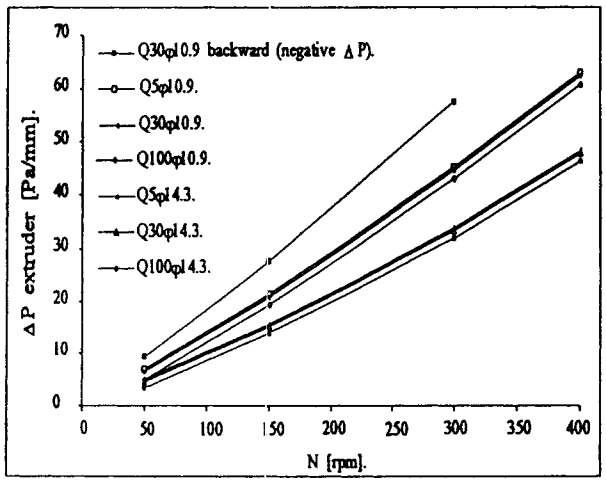

Fig. 10. The pressure buildup, ΔP, along the twin-screw extruder, η = 0.1 [Pas], Pb1.

and even necessary to have a sufficient buildup of pressure to balance, for example, the pressure drop in the die (7). For larger N, a larger difference between both helix angles is calculated. It is also found that for very small values of N, ΔP for $\varphi = 14.3°$ is larger than ΔP for $\varphi = 10.9°$ even though these values of N are not in current use in the industry. For backward elements the pressure drop is larger than the buildup, for the same Q, and the difference does not remain constant while N varies. The values are represented by the following functions (with ΔP along the extruder):

$$\Delta P[\text{Pa/mm}] = 16.05 \times 10^{-2} * N - 2.45 \times 10^{-2} * Q \quad \text{for} \quad \varphi = 10.9° \quad (11)$$

$$\Delta P[\text{Pa/mm}] = 12.29 \times 10^{-2} * N - 2.05 \times 10^{-2} * Q \quad \text{for} \quad \varphi = 14.3° \quad (12)$$

For the backward element,

$$\Delta P[\text{Pa/mm}] = 19.347 \times 10^{-2} * N - 73.41 \times 10^{-2} * Q \quad \text{for} \quad Q = 30 \text{ (ml/s)} \quad \text{and} \quad \varphi = 10.9° \quad (13)$$

The Shear and Elongation Rates

The evaluation of deformations of the polymer is important in order to understand the mixing and the heat transfer in the extruder. The two components of the deformation, the shear rate $\dot{\gamma}$ and the elongation rate $\dot{\epsilon}$, are calculated. These quantities are computed with (10):

$$\dot{\epsilon} = \frac{1}{2}(\nabla\vec{v} + \nabla\vec{v}^T):\frac{\vec{v}\ \vec{v}}{\|\vec{v}\|\|\vec{v}\|}$$

$$= (u^2u_x + v^2v_y + w^2w_z + uv(v_y + v_x) + uw(u_z + w_x) + vw(v_z + w_y))/(u^2 + v^2 + w^2) \quad (14)$$

$$\dot{\gamma} = \sqrt{2(\nabla\vec{v} + \nabla\vec{v}^T):(\nabla\vec{v} + \nabla\vec{v}^T)} = ((2u_x^2 + 2v_y^2 + 2w_z^2 + (u_y + v_x)^2 + (u_z + w_x)^2 + (v_z + w_y)^2)^{1/2} \quad (15)$$

The integral mean values of the rates in each cross section of the channel, $\bar{\dot{\gamma}}$ and $\bar{\dot{\epsilon}}$, and the integral mean values for the complete Pb1 and Pb2 ($\bar{\bar{\dot{\gamma}}}_1$, $\bar{\bar{\dot{\epsilon}}}_1$, and $\bar{\bar{\dot{\gamma}}}_2$, $\bar{\bar{\dot{\epsilon}}}_2$) are also computed. As the flow does not change along Pb1, $\bar{\dot{\gamma}}$ and $\bar{\dot{\epsilon}}$ remain constant along Pb1 and so $\bar{\bar{\dot{\gamma}}}_1 = \bar{\dot{\gamma}}$ and and $\bar{\bar{\dot{\epsilon}}}_1 = \bar{\dot{\epsilon}}$.

Figure 11 shows the evolution of $\bar{\dot{\gamma}}$ and $\bar{\dot{\epsilon}}$ along the channel for both problems. The shear and the elongation rates increase in the intermeshing area. Indeed, in the intermeshing zone, the polymer has to change direction because of the change of screw. Before and after the intermeshing region, localized axial recirculations are also found, created by the flights of the two screws.

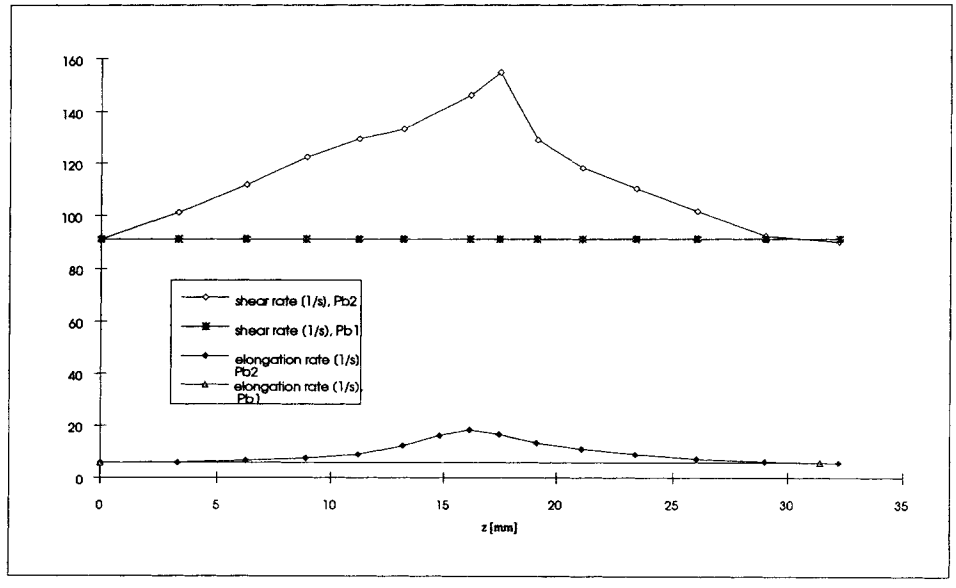

Fig. 11. Shear and elongation rates along the channel (N = 150 [rpm], Q = 30 [ml/s] and φ = 10.9°).

In *Figs. 12* and *13* the mean values for the channel, $\dot{\bar{\gamma}}$ and $\dot{\bar{\epsilon}}$, are shown for varying N and Q. The two rates increase with N and decrease with Q. This is due to the recirculation (linked to the axial backflow). The influence of N is, as for the pressure and B^*, prominent. The values for shear rate are larger than those for elongation rate. This can be related to the fact that the values of the velocity produced by N are larger than by Q and also because N has a component perpendicular to the axis of the channel. The change of φ has only a slight effect on both rates. The graphs are represented by the following functions:

$$\dot{\bar{\gamma}} = 0.8 \times 10^{-1} * N - 1.0 \times 10^{-2} * Q \quad \text{for} \quad \varphi = 10.9° \tag{16}$$

$$\dot{\bar{\epsilon}} = 5.53 \times 10^{-2} * N - 7.14 \times 10^{-3} * Q \quad \text{for} \quad \varphi = 10.9° \tag{17}$$

$$\dot{\bar{\gamma}} = 1.02 \times 10^{-1} * N - 3.5 \times 10^{-2} * Q \quad \text{for} \quad \varphi = 14.3° \tag{18}$$

$$\dot{\bar{\epsilon}} = 6.31 \times 10^{-2} * N - 8.12 \times 10^{-3} * Q \quad \text{for} \quad \varphi = 14.3° \tag{19}$$

For the backward element

$$\dot{\bar{\gamma}} = N + 11 \text{ and } \dot{\bar{\epsilon}} = 5.7 \times 10^{-2} * N - 0.72$$

$$\text{for} \quad Q = 30 \text{ (ml/s)and } \varphi = 10.9° \tag{20}$$

The Adiabatic Temperature Rise

The dissipative action of the shearing forces acting on the fluid causes a temperature rise. The shear rate values can be used to compute the viscous dissipation W by integration of $\eta\dot{\gamma}^2$ over the channel volume, for the Newtonian case. Assuming no heat leaves the extruder via the screw and barrel walls, the overall adiabatic temperature rise per unit volume is $W/(\rho C_p Q_e)$ [K/m^3] with C_p the specific heat [$C_p = 2 \times 10^3$ J/(kg·K)]. The assumption of an adiabatic temperature rise is reasonable if the volume-area ratio of the extruder volume is large, which occurs in the case of a very large diameter of the extruder.

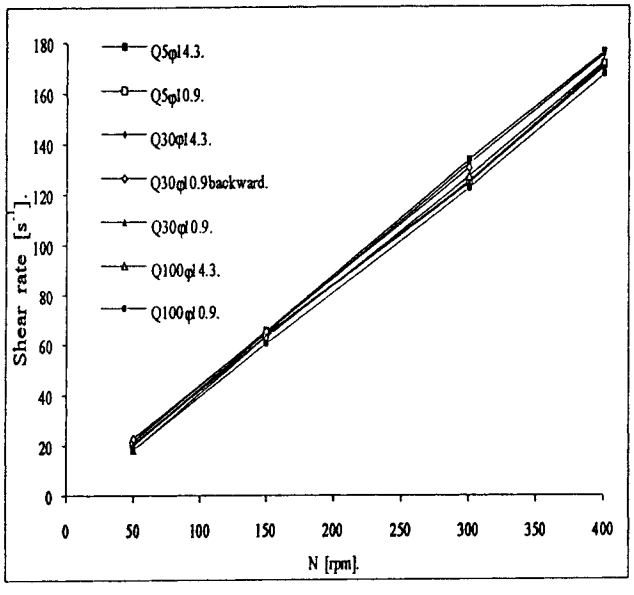

Fig. 12. Shear rate as a function of N for various values of Q and φ, Pb1.

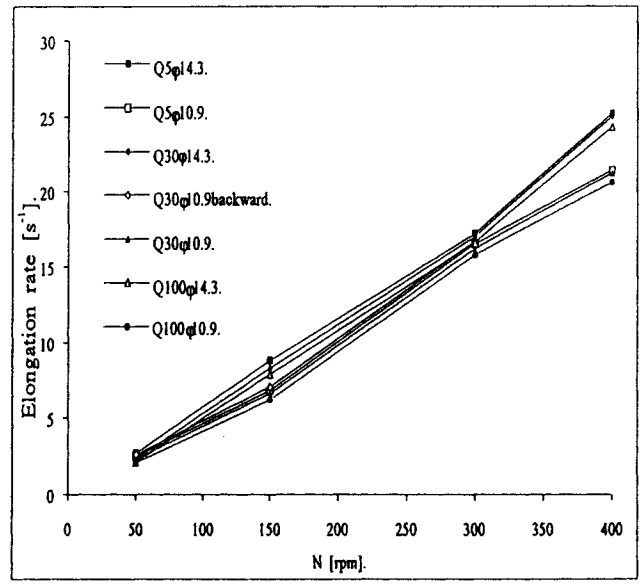

Fig. 13. Elongation rate as a function of N for various values of Q and φ, Pb1.

Figure 14 shows the temperature rise per unit length ΔT (K/mm) along the extruder for $\eta = 0.1$ (Pa.s) (see following section for the change of the viscosity). The influence of Q increases with N. The following functions represent the graph:

$$\Delta T = Q^{-1.1} * N^{2.1} * 1.5 \times 10^{-8} \quad \text{for} \quad \varphi = 10.9° \tag{21}$$

$$\Delta T = Q^{-1.1} * N^{2.1} * 2.6 \times 10^{-8} \quad \text{for} \quad \varphi = 14.3° \tag{22}$$

For the backward element, $\Delta T = N^{1.98} * 12 \times 10^{-10}$ for $Q = 30$ (ml/s), and $\varphi = 10.9°$.

It is interesting to note, from *Eqs 21* and *22*, that ΔT can be reasonably represented by a function of N^2/Q.

The Influence of Viscosity

Different materials can be used in an extruder and, during a reactive extrusion, the viscosity changes along the screws. The cases chosen to study the influence of viscosity changes are two configurations with the same value of N/Q ($N = 50$, $Q = 5$ and $N = 300$, $Q = 30$ with $\varphi = 10.9°$). The density is taken constant while the viscosity changes from 0.01 to 100 (Pa.s).

The axial pressure gradient is largely influenced by the viscosity, as shown in *Fig. 15*. The pressure buildup is almost linear in η and it can be represented by the following function, which includes N, Q, and η:

$$\Delta P = \eta^{0.98} * \left(\frac{16.05 \times 10^{-2} * N - 2.45 \times 10^{-2} * Q}{0.105} \right)$$

$$\text{for} \quad \varphi = 10.9° \tag{23}$$

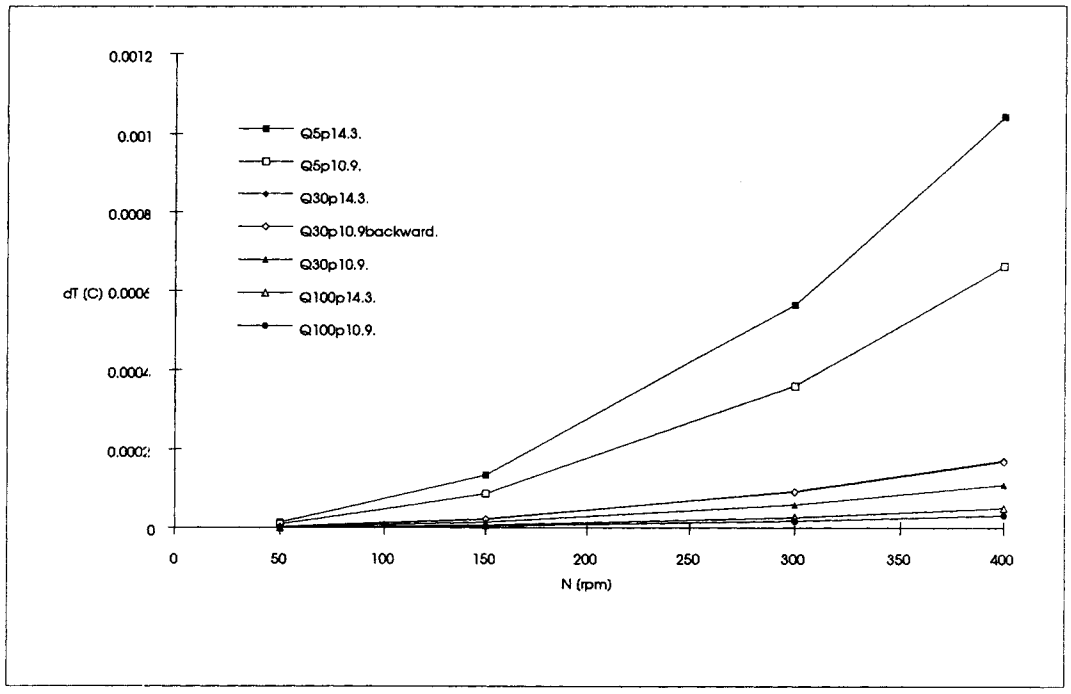

Fig. 14. The adiabatic temperature rise along the extruder as a function of N for various values of Q and φ.

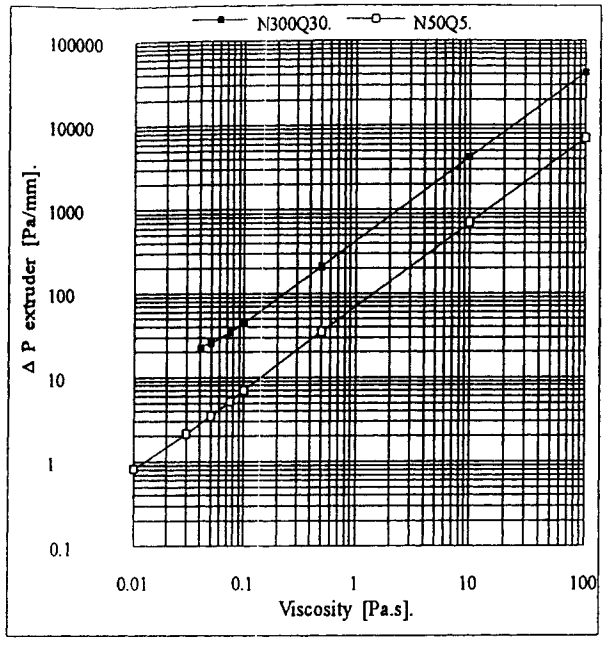

Fig. 15. The pressure buildup, ΔP, as a function of the viscosity, Pb1.

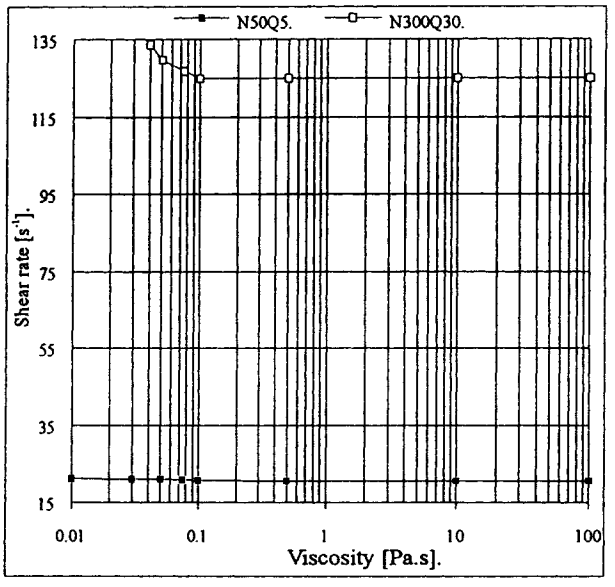

Fig. 16. Shear rate as a function of the viscosity, Pb1.

The shear and elongation rates decrease with η, especially for the small values, as shown in *Figs. 16* and *17*. The influence is stronger for the case $N = 300$ (rpm), $Q = 30$ (ml/s). Indeed, an increase of the rotation speed enlarges the Reynolds number, as does a reduction of the viscosity.

The adiabatic temperature rise ΔT (previous section) is linearly dependent on η because $\dot{\gamma}$ does almost not vary with η.

The following functions for ΔT include the viscosity:

$$\Delta T = Q^{-1.046} * "N^{1.95} * 7.26 \times (\eta * 10^{-8})$$

for $\varphi = 10.9°$ and $Re \leq 440$,

$$\Delta T = Q^{-1.038} * N^{1.95} * 6.74 \times (\eta * 10^{-8})$$

for $\varphi = 14.3°$ and $Re \leq 440$.

For the backward element, $\Delta T = N^{1.936} * 2.66 \times (\eta * 10^{-9})$ for $Q = 30$ (ml/s), $\varphi = 10.9°$, and $Re \leq 440$.

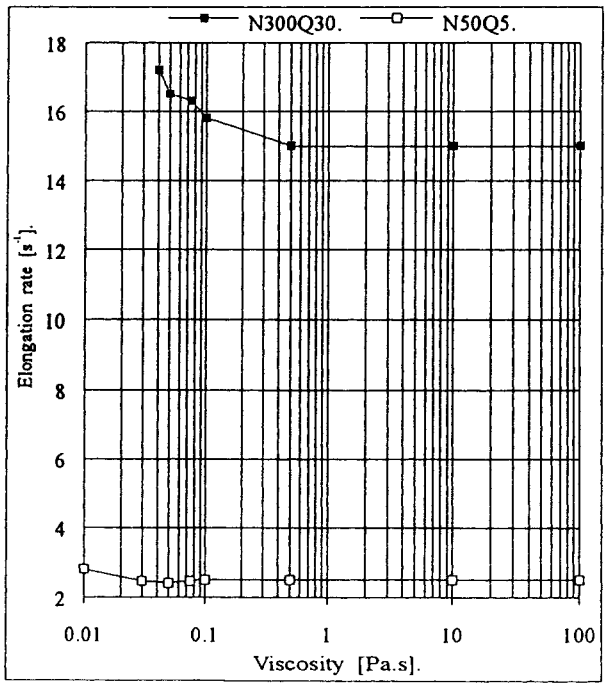

Fig. 17. Elongation rate as a function of the viscosity, Pb1.

CONCLUSIONS

This paper presents the influences of N and Q (and φ) on the buildup of pressure, the flow, the backflow volume, and the shear and elongation rates. These results are important for the optimization of melting and mixing processes in the extruder and the design of self-wiping intermeshing corotating twin-screw extruders.

It is noted that the shear and elongation rate are linked to the backflow and the pressure buildup, which are, mainly, connected to the rotation speed. These parameters (along with the throughput) influence the mixing properties of the transporting elements and the buildup of pressure necessary to pass through the kneading elements. The backflow volume also influences the residence time distribution. This backflow, which can be related to the mixing, is linked to N/Q. The shear rate is found to dominate the elongation rate by a factor 10 [the same is found in the kneading element (9)]. The adiabatic temperature rise along the extruder can be reasonably represented by a function of N^2/Q.

The results found are related to those from the companion paper Van der Wal *et al.* (9) dealing with the kneading elements, and a further discussion will be given in that paper.

ACKNOWLEDGMENT

This paper belongs to a general study on the corotating twin-screw extruder done with the collaboration of the University of Groningen the Netherlands and Elf Aquitaine (Atochem) (France). The authors would like to acknowledge the support from the C.e.r.d.a.t.o from Elf Atochem (Elf Aquitaine France). Part of this work has been supported by the foundation for chemical research in the Netherlands (SON), a division of the Dutch organization for the advancement of pure research, NWO.

NOMENCLATURE

B (ml/s) = Minus the integral, over a cross section, of the amount of flow volume in the opposite direction.
B^* (−) = B divided by Q_c.
C_L (m) = Centerline distance of the twin-screw extruder.
C_p (J/kg.K) = Specific heat.
l (mm) = Lead of screw element.
L = Divergence matrix.
M_p = Pressure mass matrix.
n (−) = Number of screw threads.
N (rpm) = Rotation speed.
$N(\tilde{u})\tilde{u}$ = Discretization of the convective terms.
p (Pa) = Pressure.
$\tilde{p}$ (Pa) = Vector of pressure unknowns.
P (Pa) = Mean pressure over a cross section.
ΔP (Pa/mm) = Buildup of pressure.
Pb1 = Geometry and mesh for the channel.
Pb2 = Geometry and mesh for the intermeshing area.
Q (ml/s) = Throughput in the extruder.
Q_e (ml/s) = Throughput in the extruder computed with the mesh.
Q_c (ml/s) = Throughput in the channel.
Re (−) = Extruder Reynolds number $\left(= \frac{2\rho V_b R_s}{\eta} \right)$.
R_s (m) = Radius of the screw.
S = Stress matrix.
ΔT (K/mm) = Adiabatic temperature rise per unit length.
$\tilde{u}$ (m/s) = Vector of velocity unknowns.
$\tilde{v}$ (m/s) = Velocity.
V_b (m/s) = Barrel velocity $\left(= \frac{2\pi R_s N}{60} \right)$.
W (Pa/s) = Viscous dissipation.
u, v, w = Components of $\tilde{v}$ (m/s).

Greek

ρ (kg/m^3) = Density of the fluid.
ϵ (m^2/Pas) = Small quantity in *Eq 5*.
η (Pas) = Dynamic viscosity.
φ (degree) = Helix angle.
$\dot{\gamma}$ (s^{-1}) = Shear rate.
$\dot{\epsilon}$ (s^{-1}) = Elongation rate.
$\bar{\dot{\gamma}}$ (s^{-1}) = Mean value of $\dot{\gamma}$ for the cross section.
$\bar{\dot{\epsilon}}$ (s^{-1}) = Mean value of $\dot{\epsilon}$ for the cross section.
$\bar{\bar{\dot{\gamma}}}$ (s^{-1}) = Mean value of $\dot{\gamma}$ for the channel.
$\bar{\bar{\dot{\epsilon}}}$ (s^{-1}) = Mean value of $\dot{\epsilon}$ for the channel.

REFERENCES

1. Sepran Package, Ingenieursbureau SEPRA, The Netherlands (1992).

2. Y. Wang and J. L. White, *J. Non-Newton. Fluid Mech.*, **32,** 19 (1989).
3. C. Cuvelier, A. Segal, and A. A. van Steenhoven: *Finite elements and Navier-Stokes equations*, D. Reidel Publishing Co., Dordrecht, The Netherlands (1986).
4. M. L. Booy, *Polym. Eng. Sci.*, **18,** 973 (1978).
5. C. D. Denson and B. K. Hwang, Jr., *Polym. Eng. Sci.*, **20,** 965 (1980).
6. W. M. Davis, *Chem. Eng. Progress*, November 1988, p. 35.
7. D. M. Kalyon, C. Jacob, and P. Yaras, *Plast. Rubb. Compos. Process. Applications*, **16,** 193 (1991).
8. Z. Chen and J. L. White, *SPE ANTEC Tech. Papers*, **38,** 1332 (1992).
9. D. J. van der Wal, E. M. Klomp, D. Goffart, H. W. Hoogstraten and L. P. B. M. Janssen, *Polym. Eng. Sci.*, this issue.
10. J. M. Ottino, *Chem. Eng. Sci.*, **35,** 1377 (1980).